Optical Engineering

OpticalEngineering.SPIEDigitalLibrary.org

Modeling multilayer coating profiles with defects on EUV collector with grating

Shizhuang Sun
Chunshui Jin
Bo Yu
Tao Guo
Shun Yao
Wenyuan Deng
Chun Li

SPIE.

Shizhuang Sun, Chunshui Jin, Bo Yu, Tao Guo, Shun Yao, Wenyuan Deng, Chun Li, "Modeling multilayer coating profiles with defects on EUV collector with grating," *Opt. Eng.* **58**(10), 107102 (2019), doi: 10.1117/1.OE.58.10.107102.

Downloaded From: https://www.spiedigitallibrary.org/journals/Optical-Engineering on 23 Jun 2020
Terms of Use: https://www.spiedigitallibrary.org/terms-of-use

Optical Engineering 58(10), 107102 (October 2019)

Modeling multilayer coating profiles with defects on EUV collector with grating

Shizhuang Sun,[a,b] Chunshui Jin,[a,*] Bo Yu,[a,b] Tao Guo,[a] Shun Yao,[a] Wenyuan Deng,[a] and Chun Li[a]
[a]Chinese Academy of Sciences, Changchun Institute of Optics, Fine Mechanics and Physics, State Key Laboratory of Applied Optics, Changchun, China
[b]University of Chinese Academy of Sciences, Beijing, China

Abstract. Extreme ultraviolet lithography (EUVL) is recognized as a leading technology in next-generation lithography. Achieving spectral purification while ensuring extreme ultraviolet (EUV) reflectance is one of the key technologies for industrializing EUVL. An EUV collector mirror with phase grating can be used in the spectral purification of an EUVL source. However, it also induces a considerable loss of EUV. We propose a deposition model for calculating the multilayer coating profile on the surface of an EUV collector with grating based on a geometric line tracing method. In addition, it also analyzes the coating defects that influence the EUV reflectance, and the evolution of the coating defects with the grating positions. Experimental results reveal that the model accurately predicts the multilayer coating profile deposited on the surface of the collector, which helps improve how EUV collector is deposited. © *2019 Society of Photo-Optical Instrumentation Engineers (SPIE)* [DOI: 10.1117/1.OE.58.10.107102]

Keywords: EUV collector with grating; multilayer coating profile; coating defects; deposition model; EUV reflectance.

Paper 190770 received Jun. 4, 2019; accepted for publication Sep. 17, 2019; published online Oct. 18, 2019.

1 Introduction

The increasing demand for low-power, high-performance electronic devices has caused the advancement of integrated circuit techniques to 10-nm technology, which has driven the development of next-generation lithography research. Extreme ultraviolet lithography (EUVL) is recognized as the leading technology in realizing the industrialization of this 10-nm technology. High-power laser-produced plasma (LPP) light sources are usually implemented as inputs for the EUVL. Extreme ultraviolet (EUV) light is generated by a 10.6-μm wavelength high power pulsed CO_2 laser exciting a Sn target. However, the EUV light energy conversion efficiency of an LPP source is less than 6% and the output power is limited. Furthermore, the output contains a large amount of infrared radiation (IR) that would increase the thermal load of the system. Therefore, removing IR from the EUV light source without affecting the EUV collection efficiency would promote the industrialization of EUVL technology.[1–7]

Global research on this has focused on the spectral purification of EUV light sources.[7] The primary structures currently employed to filter IR from EUV sources include transmissive thin film filters, reflective gratings, and collector mirrors with gratings. Transmission grating, which is a filter structure used by the firm ASML Holding from 2010 to 2011, consists of Zr and $ZrSi_2$ and is ~90 nm thick. It has a transmittance of 65% for EUV light and can also effectively absorb IR.[8,9] In 2009, the FOM Institute for Plasma Physics Rijnhuizen designed a blazed grating with a blaze angle of 21 deg that effectively diffracted and filtered IR and had a 68% reflectivity for EUV light.[10] In 2014, FOM Labs produced a pyramid-type grating filter that scatters infrared and ultraviolet light.[11] In 2014, Rigaku Corp. designed a collector mirror with a phase grating that effectively scattered 10.6-μm infrared-driven lasers while maintaining a high EUV collection efficiency.[12] In 2015, the IOF laboratory in Germany designed an EUV collector with a dual-wavelength spectral purity filter. The double-layer grating structure of the collector mirror effectively scattered 10.6 μm to achieve the spectral purification of the EUV source.[13]

These methods of spectral purification suppress the IR energy in a light source to less than 1%, which satisfies the spectral purification requirement. However, the transmissive thin film filter, transmission grating, and reflective grating structure account for an ~30% loss in EUV,[7–11] which substantially limits increases in the output power of the EUV source. However, the collector with phase grating has an EUV loss of ~4.81%;[12,13] therefore, it is more valuable to explore this structure than the others.

According to research and analysis on multilayer coatings on an EUV collector, this loss of EUV reflectance may be attributed to the coating defects at the groove edges and the increased high-spatial frequency roughness of the collector compared to an Si wafer with an extremely low sub-angstrom roughness.[13] However, the effect of these two factors on the EUV reflectance from a collector mirror has not been discussed. Therefore, we establish a deposition model to study the influence of coating defects on EUV reflectivity. It can be used to simulate the deposition on large-scale curved grating to aid in further research on improving its diffraction efficiency. Furthermore, because it is a general model, it can also be used to simulate depositions on gratings for visible and ultraviolet light. It would be mainly applied in determining coating profiles, which helps in EUV spectroscopy analysis of coated gratings.[14] We tested the model in an experiment in which a Mo/Si multilayer coating was deposited on phase grating via magnetron sputtering. The cross-section of the phase grating was then measured with focused ion beam and transmission electron microscopy. The experiment verified the accuracy of the coating simulation model.

*Address all correspondence to Chunshui Jin, E-mail: jincs@sklao.ac.cn

0091-3286/2019/$28.00 © 2019 SPIE

Downloaded From: https://www.spiedigitallibrary.org/journals/Optical-Engineering on 23 Jun 2020
Terms of Use: https://www.spiedigitallibrary.org/terms-of-use

2 Extreme Ultraviolet Collector Mirror with Spectral Purification

This section details how the structure parameters of the collector and the surface grating were calculated. These parameters were used to simulate the deposition process on the collector mirror with phase grating.

The structure of the designed collector mirror (Fig. 1) is ellipsoidal and 600 mm in diameter, with the Sn plasma excitation located near the focus of the collector, i.e., 200 mm away from the center of the collector mirror. The EUV light enters the lighting system from the other focus.[8] The collection angle of the collector is 5 sr.

To achieve the purpose of filtering out 10.6 μm IR, a phase grating [shown in Fig. 2(b)] with a period of 1 mm, depth of 2.75 μm, and a duty ratio of 50% was designed according to the IR diffraction function shown in Eqs. (1–3) below:[15,16]

$$\alpha = \arcsin\left(m\frac{\lambda}{\Lambda}\right), \tag{1}$$

$$\delta r = L \cdot \tan\left[\arcsin\left(m\frac{\lambda}{\Lambda}\right)\right], \tag{2}$$

$$d = \lambda/4, \tag{3}$$

where Λ is the period of the grating, λ is the wavelength of the incident light, n is the diffraction order, θ_n is the diffraction angle, and θ is the incident angle.

This design ensures that the structure achieves the maximum diffraction efficiency for IR.

To realize the purpose of reflecting EUV light, it is also necessary to deposit a Mo/Si multilayer coating on the surface of the collector.[1] According to previous research,[13] a collector mirror without a grating has a reflectivity of approximately 69% for EUV light, but after placing a grating on the collector mirror the reflectance of the collector mirror is reduced to 64%. To deal with the decrease in EUV reflectivity, this study used a geometric line tracing method to simulate the deposition of sputtering particles on the phase grating and investigate the influence of the coating defects on EUV reflectivity.

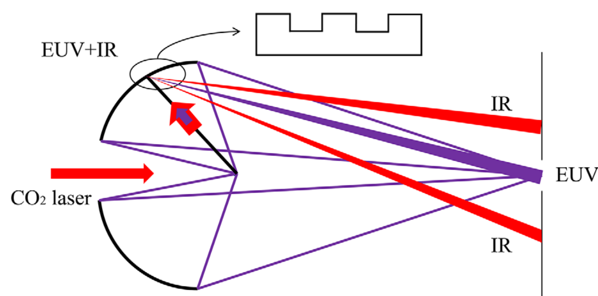

Fig. 1 EUV collector mirror with grating.

3 Simulations of the Deposition of Multilayer Coating Using a Geometric Line Tracing Method

A block judgment algorithm for the coating on the phase grating was established based on the geometric line tracing method[17] and the relative motion of the target and the collector. Therefore, a deposition model of the multilayer coating on the phase grating was established. In addition, the coating profile was evaluated, and the coating defect was further explored.

3.1 *Simulation Hypotheses of the Deposition Process*

There are three hypotheses regarding the deposition process of sputtered particles, based on Yu et al.:[18] initial distribution, flying process in the air, and deposition on the collector. They are described below.

1. Initial distribution. This hypothesis suggests that the distribution of particles sputtered by the magnetron sputtering source is only related to the target structure and does not change with time.
2. Flying process in the air. This hypothesis suggests that the working gas pressure of the magnetron sputtering deposition process is generally below the order of 1 mtorr. It also suggests that the distance between the target and the collector is ~100 mm, and therefore, the interaction of the sputtered particles with the gas particles can be disregarded. The sputtered particles are deposited directly onto the collector.
3. Deposition on a collector. This hypothesis suggests that when the particles are deposited on the surface of the collector, their viscosity coefficient is considered to be 1; i.e., all particles are deposited onto the collector to form the multilayer coating. The lateral displacement of the particles on the substrate and the secondary sputtering of the particles on the substrate are not considered.

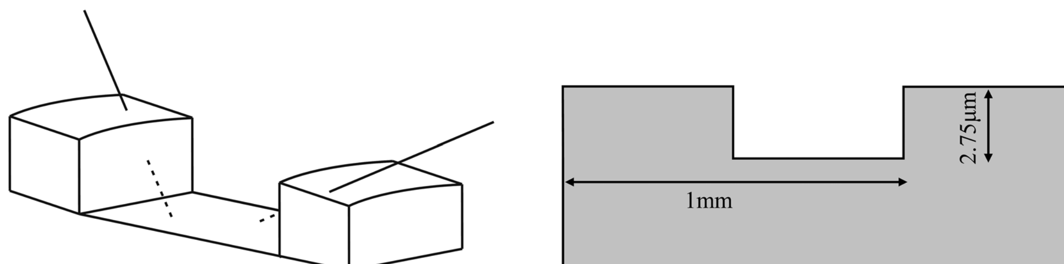

Fig. 2 (a) Blocking situation when the coating particles are blocked by the sidewall of the grating and (b) structure of the grating.

Downloaded From: https://www.spiedigitallibrary.org/journals/Optical-Engineering on 23 Jun 2020
Terms of Use: https://www.spiedigitallibrary.org/terms-of-use

3.2 *Simulating the Multilayer Deposition on the Grating*

This section describes the model established for multilayer deposition on the grating based on the three hypotheses mentioned in Sec. 3.1 in combination with the relative motion between the collector and the target.

3.2.1 *Motion of the collector relative to the target*

The position of the collector relative to the target depends on the revolution and rotation of the collector, which in turn is based on the structure of the magnetron sputtering.[19] Therefore, the change in the relative position over time can be determined by the angular velocity of the revolution ω and the angular velocity of the rotation ω_s, as shown in Fig. 3.

The planetary motion trajectory at point S (Fig. 4) on the collector can be described as

$$x_s = R\cos(\theta) - R + r\cos\varphi, \tag{4}$$

$$y_s = R\sin(\theta) + r\sin\varphi, \tag{5}$$

$$z_s = h(r), \tag{6}$$

where θ is the revolution angle, φ is the rotation angle, $\theta = \omega t + \theta_0$; $\varphi = \omega_s t + \varphi_0$, R is the revolution radius (the distance from the rotation axis to the revolution axis), and r is the distance from the point S to the rotation center on the collector.

The trajectory of a point on the collector can be calculated using Eqs. (4)–(6), and the model of the relative motion of the target to the collector can also be established.

3.2.2 *Film growth on the collector*

The position of the collector relative to the target during sputtering is shown in Fig. 4. The sputtering rate of a certain pixel dA_T on the target to point S on the collector is[20] $D = p(\alpha)\cos(\beta)/\rho^2$, where α is the angle between the exiting direction $\vec{TS}$ and the normal direction of the target for the sputtered particles and $p(\alpha)$ is the angular distribution function of the sputtered particles. For magnetron sputtering,[21,22] $p(\alpha) = \cos(\alpha)^n$, where β is the angle between $\vec{TS}$ and the normal direction on point S on the collector, ρ is the distance from the point S to the point T, $\rho = |\vec{ST}|$, $\cos(\alpha) = h/\rho$, $\cos(\beta) = (\vec{ST}\cdot\hat{n})/\rho$, h is the vertical distance from the

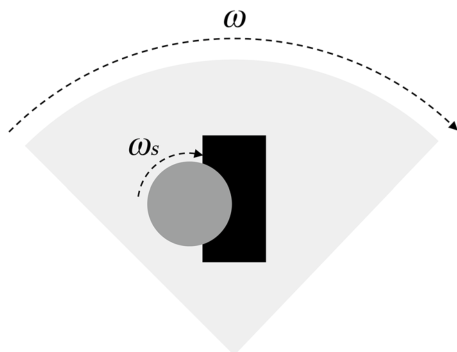

Fig. 3 Motion of the collector relative to the target.

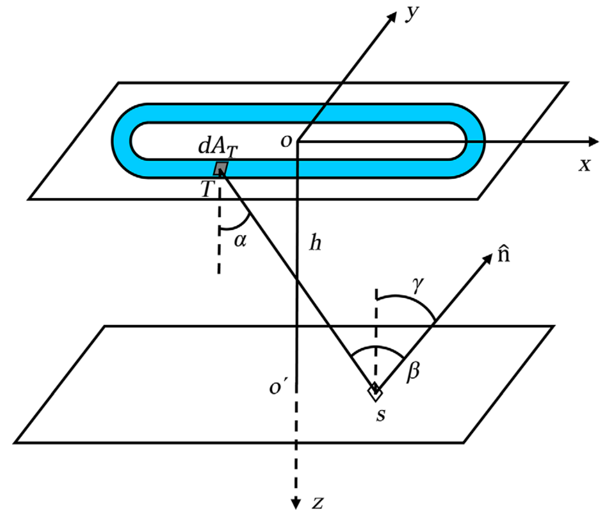

Fig. 4 Relative structures and parameters of sputtered particles, the target, and the collector.

target to the collector, and $\hat{n}$ is the unit normal vector on the collector.

The relationship between the unit normal vector and the rotation angle φ is expressed as follows:

$$\hat{n} = (\cos\varphi\sin\gamma, \sin\varphi\sin\gamma, -\cos\gamma), \tag{7}$$

where γ is the angle between the unit normal vector and the z-axis. For a concave surface, $-\pi/2 < \gamma < 0$ and for a convex surface, $0 < \gamma < \pi/2$. The weighted integral of the deposition at point S from the entire planar target is

$$T(r) = \iint \mathrm{d}A_T \int D(x_T, y_T)\frac{\cos^k(\alpha)\cos(\beta)}{\rho^2\omega(\theta)}\mathrm{d}\theta, \tag{8}$$

where $D(x_T, y_T)$ is the yield distribution of the sputtered particles from the target.[23] According to this equation, the deposition thickness from the entire sputtering target at point S can be obtained.

The coating model can be designed using the previous steps. However, because the block of the sputtered particles by the grating is not considered, a block judgment algorithm is added to establish a new coating model for the EUV collector.

3.3 *Block Judgment Algorithm*

When the particles are deposited onto the upper bottom surface of the grating, they would not be blocked by the phase grating. However, when they are deposited onto the lower bottom surface of the grating, they may be blocked by the sidewall of the grating and form a defect region. These coating defects reduce the EUV reflection efficiency on collector. A schematic of the sidewall blocking particles is given in Fig. 2(a).

The block judgment algorithm works as follows:

1. In the magnetron sputtering coating process, the velocity of the sputtered particles is higher than the velocity of the collector. Therefore, sputtered particles can be considered to be deposited from the sputter target onto the collector in a linear path.

Downloaded From: https://www.spiedigitallibrary.org/journals/Optical-Engineering on 23 Jun 2020
Terms of Use: https://www.spiedigitallibrary.org/terms-of-use

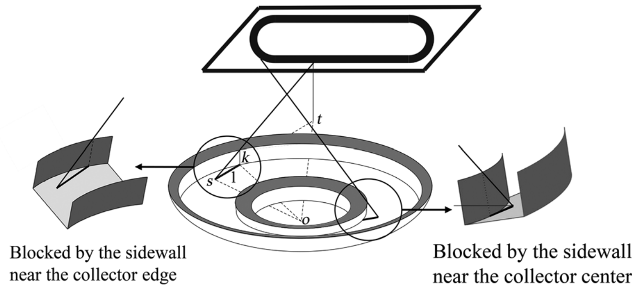

Fig. 5 Two types of blocks caused by the two sidewalls.

2. The trajectory of the sputtered particles determines which side is blocked. The lengths of the flight paths of the sputtered particles projected on the lower bottom of the gratings are calculated separately. If they are blocked by the sidewall near the collector center, the equation is as follows (Fig. 5):

$$l = os \times \cos \angle tso - \sqrt{(os \times \cos \angle tso)^2 - os^2 + ok^2}. \tag{9}$$

However, if they are blocked by the sidewall near the collector edge, this equation is used:

$$l = \mathrm{abs}(os \times \cos \angle tso) + \sqrt{(os \times \cos \angle tso)^2 - os^2 + ok^2}. \tag{10}$$

3. The distance SS_1 (Fig. 6), which is the distance from point S to the sidewall, can be obtained based on the position of point S. The vertical height difference h_1 between point S and point S_1 can be calculated based on the inclination angle of the collector at point S. After this, the angle β_1 can be calculated based on l and h_1.

$$h_1 = SS_1 \times \sin(\beta), \tag{11}$$

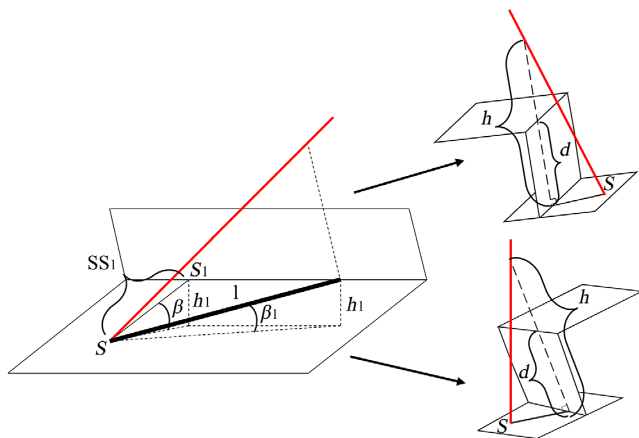

Fig. 6 (a) Vertical projection and angles of the flight path of the sputtered particles; (b) vertical projection of the flight path on the sidewall near the center; and (c) vertical projection of the flight path on the sidewall near the edge.

$$\beta_1 = \arcsin\left(\frac{h_1}{l}\right). \tag{12}$$

The calculation of the projection height h also requires consideration of the sidewall near the collector center and sidewall near the collector edge. The angle β_2 between the flight path and the horizontal plane can be calculated by the angle between S and the target, after which the height h can be calculated as follows for the sidewall near the collector center:

$$h = l \times \tan(\beta_1 + \beta_2), \tag{13}$$

and as below for the sidewall near the collector edge:

$$h = l \times \tan(\beta_2 - \beta_1). \tag{14}$$

After these are calculated, h is compared with depth d. If $h > d$, the sputtered particles are not blocked. If $h \le d$, the sputtered particles are blocked.

Finally, the multilayer coating deposition equation can be derived in Eq. (15) and then used in the simulation coating model:

$$T(r) = \iint \mathrm{d}A_T \int M \times D(x_T, y_T) \frac{\cos^k(\alpha)\cos(\beta)}{\rho^2 \omega(\theta)} \mathrm{d}\theta. \tag{15}$$

The parameter M is the blocking judgment operator. If the sputtered particles are blocked (i.e., if $h < d$), $M = 0$. If the sputtered particles are not blocked (i.e., if $h > d$), $M = 1$.

It is worth noting that just like the calculation of particle deposition on the lower bottom surface, the simulation of deposition on the grating sidewall also needs to introduce the parameter M. Whether the sputtered particles are blocked or not is determined by the angle of the flight path with sidewall.

3.4 *Establishing a Simulation Deposition Model*

Equation (15) demonstrates how sputtered particles are deposited on the collector mirror when they are blocked. This data can be used to establish a simulation deposition model.

The simulation of the deposition on the collector is shown in Fig. 7. First, according to the position of the sputtered particles, we can determine whether the particles are deposited on the upper bottom surface or the lower bottom surface of the grating. If the particles are deposited on the upper bottom surface, the thickness of the multilayer coating is calculated using Eq. (8). However, if the particles are deposited on the lower bottom surface, the thickness of the multilayer coating is calculated according to Eq. (15). Therefore, given these calculation processes, a simulation model can be established for deposition on the collector mirror taking coating defects into account.

The model can simulate the multilayer coating profile on the phase grating and then calculate the defect region. The surface roughness of the multilayer coating (rms) should be less than 0.7 nm to meet high reflectivity requirements.[24] Therefore, when the thickness of a film region is less than

Downloaded From: https://www.spiedigitallibrary.org/journals/Optical-Engineering on 23 Jun 2020
Terms of Use: https://www.spiedigitallibrary.org/terms-of-use

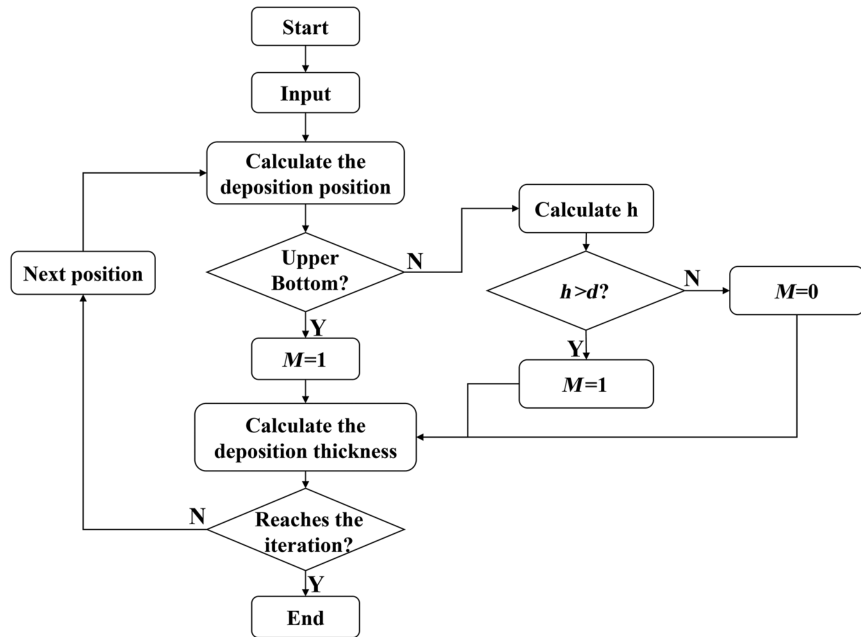

Fig. 7 Flowchart of the simulation model.

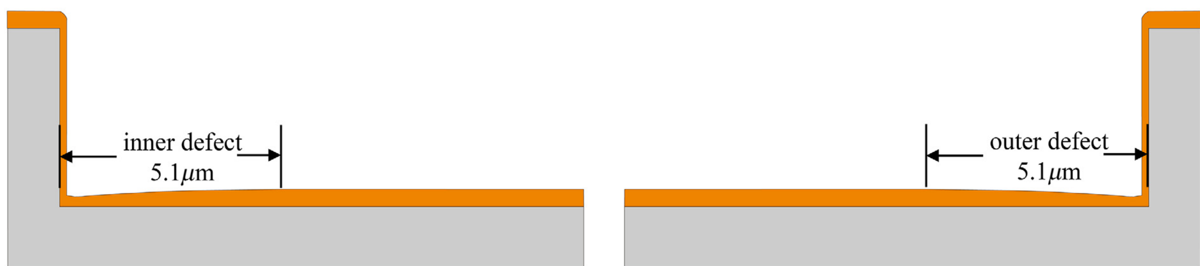

Fig. 8 (a) Coating profile and inner defect when the sidewall is near the center of the collector mirror and the inner defect is the defective area of interest. (b) Coating profile and outer defect when the sidewall is near the edge of the collector mirror and the outer defect is the defective area of interest. The gray region is the grating and the yellow region is the multilayer coating.

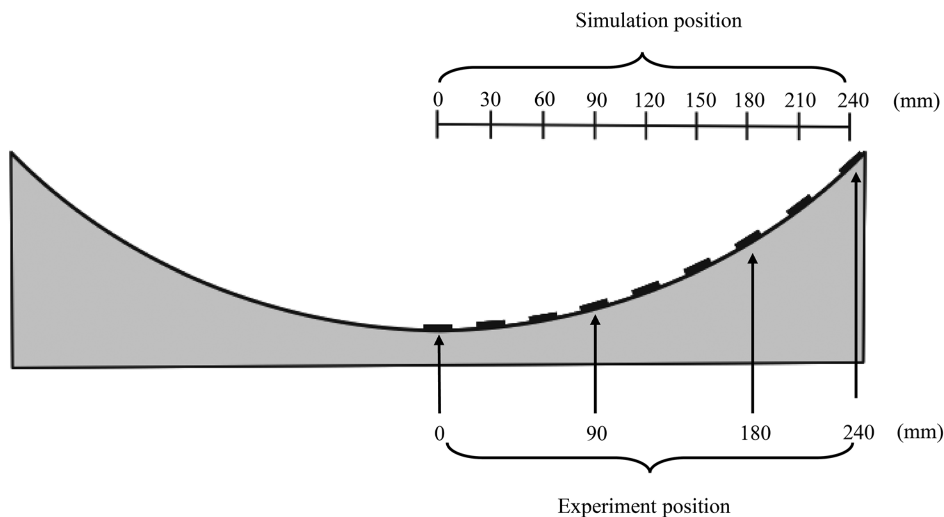

Fig. 9 Grating locations in the simulation and experiment in this study.

Downloaded From: https://www.spiedigitallibrary.org/journals/Optical-Engineering on 23 Jun 2020
Terms of Use: https://www.spiedigitallibrary.org/terms-of-use

0.7 nm compared to the normal film, the former is regarded as defective. This allows defective regions of the multilayer coating on the EUV collector to be located and the influence of coating defects on the reflectivity of the collector mirror to be studied further.

4 Simulation and Experiment Results

This section details the characterization of the multilayer coating profile on the collector mirror with grating. The coating defect variation with the grating position is revealed and correlated.

4.1 *Simulation Results of the Multilayer Coating When the Grating is Located in the Center of the Collector*

Figure 8 shows the simulation results of the coating on a grating located in the center of the collector. There are no coating defects on the upper bottom surface although there are

Grating position s (mm)	Defect situations	Simulation multilayer film profile	Defect length (μm)	Experiment multilayer film profile	Defect length (μm)
0	inner defect		5.10		5.00
	outer defect		5.10		5.00
90	inner defect		4.81		4.42
	outer defect		6.54		6.20
180	inner defect		3.31		3.24
	outer defect		8.13		7.71
240	inner defect		2.87		2.88
	outer defect		11.2		10.76

Fig. 10 Simulation and experiment result of multilayer coating profile and defect length when gratings are 0, 90, 180, and 240 mm from the center of the collector.

Downloaded From: https://www.spiedigitallibrary.org/journals/Optical-Engineering on 23 Jun 2020
Terms of Use: https://www.spiedigitallibrary.org/terms-of-use

obvious defects near the sidewall on the lower bottom surface. Each defect region is 5.10 μm in length, the total length of the two defect regions is 10.2 μm. The period of the grating is 1 mm shown in Fig. 2(b). Therefore, it can be inferred that the defect region accounts for ~1.02% of the period of a grating.

4.2 *Simulation Results of the Multilayer Coating When the Gratings are Located in Different Locations*

We selected four different grating positions, 0, 90, 180, and 240 mm from the center of the collector mirror (Fig. 9), and the results obtained from the simulation are shown in Fig. 10.

By comparing the simulation results in Fig. 10, the following observations can be made:

1. The coating surface on the upper bottom of the grating is extremely smooth because no blocking is caused by the sidewall, and an arc-shaped convex defect at the boundary between the sidewall and the upper bottom is observed.
2. The profile of the multilayer coating changes when the grating position changes, as shown in the third column. For the inner defect, the defect length decreases as the grating position increases; for the outer defect, the defect length increases as the grating position increases. The reasons for this phenomenon are as follows: (a) there are more sputtered particles with a small incident angle and (b) fewer particles are blocked with the increase of grating position when the sidewall is near the center of the collector center, thus decreasing the defect length. When the sidewall is near the collector edge, more particles are blocked as the grating position increases, thus increasing the defect length.
3. There is also a film deposited on the sidewall of the grating in the third column of Fig. 10. The thickness of the film on the sidewall is thinner than that of the film on the lower bottom surface. For the inner defects, the thickness of the film deposited on the sidewall increases as the grating position increases. For the outer defects, the thickness of the film deposed on the sidewall decreases with increases in grating position. The thickness of the film on the sidewall is also much thinner than the length of coating defect on the lower bottom surface. Therefore, it is considered that the film deposited on the sidewall does not influence EUV reflectance.

4.3 *Experimental Results of the Multilayer Coating When the Gratings are Located in Different Locations*

The experiment was conducted under a DC magnetron sputtering system "Nessy 1900" produced by Leybold Optics (Fig. 11). A detailed description of the system can be found in Refs. 18 and 25. The vacuum chamber had a diameter of 1900 mm, and the vacuum pump used was a cryopump. Six rectangular targets of dimensions 600 mm × 125 mm were radially distributed in the chamber, and the substrates that could be rotated were held under the targets. The process gas

Fig. 11 DC magnetron sputtering system "Nessy 1900."

was argon, and the working pressure was 8E-4 mbar. We used four grating slices placed at different positions with an ellipsoidal base as the collector mirror (Fig. 9). The slices were square phase gratings 15 mm × 15 mm in size, with a period of 1 mm, a depth of 2.75 μm, and a duty ratio of 50%. The structure of the experimental grating is shown in Fig. 12. The Mo/Si multilayer coatings with 50 bilayers (period) were deposited on the gratings. The results of the multilayer coating profile are shown in the fifth column of Fig. 10.

By comparing the experiment results with the simulation results in Fig. 10, the following conclusions can be made.

1. The multilayer coating surface on the upper bottom of the grating is very smooth. The experimental results are the same as the simulation results and almost no coating defects were generated.
2. There were significant variations in the thickness of the film at the lower bottom surface near the sidewall, which is regarded as a coating defect in the simulation model. How this varies with the grating position is the same as how it varies in the simulation.
3. There is also a film deposition on the surface of the sidewall that is identical to the result in the simulation. The film deposited on the sidewall is much thinner than the coating defect length on the lower bottom surface. Thus, it can be considered that the film deposited on the sidewall does not affect EUV reflectance.
4. There is an arc-shaped convex defect at the boundary between the sidewall and the upper bottom. A similar structure can be seen in the simulation results and the simulated coating profile agrees with the experimental results.

4.4 *Modeling of Coating Defect*

Figure 13 shows the variation in the defect length with the grating position. As shown in Fig. 13(a), for the inner defect, the defect length decreases with the increase in the grating position. These correlate well with the quadratic equation $d \sim -r^2$. This is because the grating is located in the ellipsoid collector, which leads the incidence angle to change with the grating positions in a quadratic correlation. Because the defect lengths are affected by the incidence angles, the variations in defect length are correlated with the grating positions by a quadratic equation. For the outer defect, the defect

Downloaded From: https://www.spiedigitallibrary.org/journals/Optical-Engineering on 23 Jun 2020
Terms of Use: https://www.spiedigitallibrary.org/terms-of-use

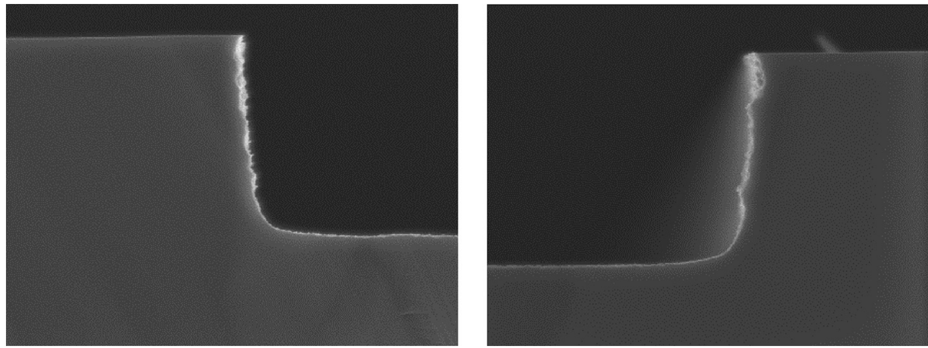

Fig. 12 Sectional view of the gratings under a scanning electron microscope.

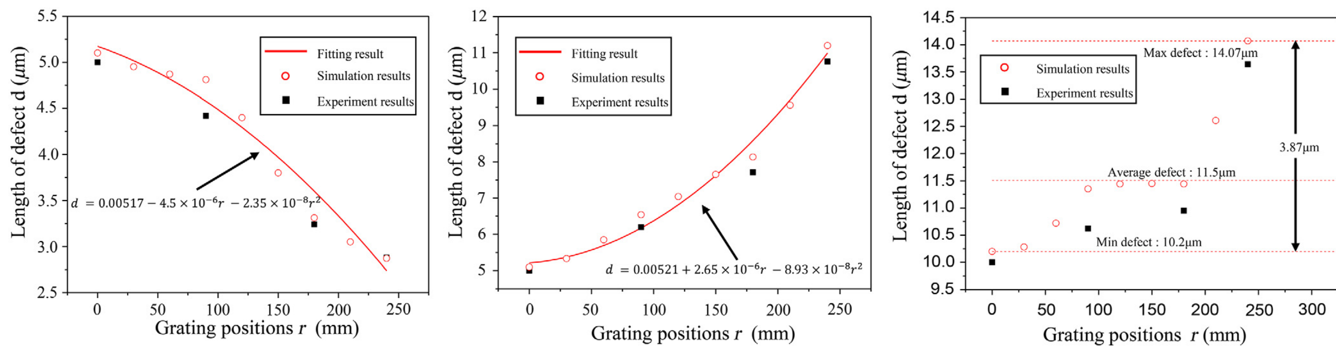

Fig. 13 Defect length variation to grating positions. (a) Inner defect, (b) outer defect, and (c) sum of inner defect and outer defect. The results from the simulation and the experiment are indicated by the red dots and the black squares, respectively.

length increases with the increase in grating position, as shown in Fig. 13(b). The evolution of the defect length with the increase in grating positions is also correlated with the quadratic equation $d \sim r^2$. Figure 13 shows that the length of the coating defect on the lower bottom surface obtained in the simulation is almost the same as that obtained in the experiment. The evolution of the position of the grating obtained from the experiment is also the same with that obtained in the simulation. The variation of the sum of the inner and outer defect length with grating positions is shown in Fig. 13(c). The sum increases slightly with increases in grating position; the gap between the maximum and minimum defect is very low, which means that the variation in the sum is too small to be considered. The average length of the sum is 11.5 μm; which suggests that the defect region accounts for 1.15% of the whole grating on average.

4.5 *Summary*

Section 4 characterized the profile of the coating deposited on the grating via a simulation model and an experiment. The evolution of the defect lengths given changes in grating position were correlated by the formula $d \sim -r^2$ for inner defects and $d \sim r^2$ for outer defects.

5 Conclusions

This paper establishes a deposition model for sputtering particles on the surface of an EUV collector with grating and reveals defects in coating. Major conclusions include the following:

1. The establishment of a model for simulating the process of film deposition on the grating of an EUV collector via geometric line tracing method. The simulation model has been verified experimentally.
2. The coating profile on the gratings was characterized, and it was found that the upper bottom surface was very smooth, whereas the lower bottom surface had obvious defects that would influence EUV reflectance. The sidewalls are also coated, but the coatings are quite thin compared to the coating defect length on the lower bottom surface. This implies that the sidewall film has little effect on EUV reflectance.
3. Both inner and outer defects were studied, and the lengths of both coating defects are quantified. Their evolution given the grating position was found to be correlated to $d \sim -r^2$ for the inner defect and $d \sim r^2$ for the outer defect.
4. The coating defect accounts for a 1.15% loss in EUV reflectance on average. Therefore, they do not account for the main reason for EUV loss in collector mirrors with gratings.
5. This model can be used to simulate coatings on large-scale curved surfaces and contribute to further research on improving their diffraction efficiency. It is also a general model that can be used to simulate coatings on gratings used for visible and ultraviolet light.

Acknowledgments

This work was supported by the National Natural Science Foundation of China (NSFC) under Grant No. 61605201.

Downloaded From: https://www.spiedigitallibrary.org/journals/Optical-Engineering on 23 Jun 2020
Terms of Use: https://www.spiedigitallibrary.org/terms-of-use

References

1. D. Attwood, *Soft X-Rays and Extreme Ultraviolet Radiation: Principles and Applications*, Cambridge University Press, Cambridge (2000).
2. E. Louis et al., "Nanometer interface and materials control for multilayer EUV-optical applications," *Prog. Surf. Sci.* **86**(11–12), 255–294 (2011).
3. C. Wagner and N. Harned, "EUV lithography: lithography gets extreme," *Nat. Photonics* **4**(1), 24–26 (2010).
4. D. C. Brandt et al., "LPP EUV source development for HVM," *Proc. SPIE* **6517**, 65170Q (2007).
5. H. Kinoshita et al., "Soft x-ray reduction lithography using multilayer mirrors," *J. Vac. Sci. Technol. B* **7**(6), 1648–1651 (1989).
6. D. C. Brandt et al., "CO_2/Sn LPP EUV sources for device development and HVM," *Proc. SPIE* **8679**, 86791G (2013).
7. W. A. Soer, "Grid spectral purity filters for suppression of infrared radiation in laser-produced plasma EUV sources," *Proc. SPIE* **7271**, 72712Y (2009).
8. N. I. Chkhalo et al., "Influence of annealing on the structural and optical properties of thin multilayer EUV filters containing Zr, Mo, and silicides of these metals," *Proc. SPIE* **7521**, 752105 (2010).
9. V. V. Medvedev et al., "Infrared suppression by hybrid EUV multilayer—IR etalon structures," *Opt. Lett.* **36**(17), 3344–3346 (2011).
10. A. J. R. van den Boogaard, "Optical element for full spectral purity from IR-generated EUV light sources," *Proc. SPIE* **7271**, 72713B (2009).
11. Q. Huang et al., "High efficiency structured EUV multilayer mirror for spectral filtering of long wavelengths," *Opt. Express* **22**(16), 19365–19374 (2014).
12. M. Kriese et al., "Development of an EUVL collector with infrared radiation suppression," *Proc. SPIE* **9048**, 90483C (2014).
13. T. Feigl et al., "Sub-aperture EUV collector with dual-wavelength spectral purity filter," *Proc. SPIE* **9422**, 94220E (2015).
14. D. L. Voronov et al., "A 10,000 groove/mm multilayer coated grating for EUV spectroscopy," *Opt. Express* **19**(7), 6320–6325 (2011).
15. T. W. Barbee, Jr., "Combined microstructure x-ray optics," *Rev. Sci. Instrum.* **60**(7), 1588–1595 (1989).
16. T. W. Barbee, "The use of multilayer diffraction gratings in the determination of x-ray, soft x-ray, and VUV elemental scattering cross-sections," *Proc. SPIE* **0911**, 169–177 (1988).
17. J. A. Thornton, "High rate thick film growth," *Annu. Rev. Mater. Sci.* **7**(1), 239–260 (1977).
18. B. Yu et al., "Control of lateral thickness gradients of Mo–Si multilayer on curved substrates using genetic algorithm," *Opt. Lett.* **40**(17), 3958–3961 (2015).
19. T. Foltyn, "Deposition of multilayer mirrors with arbitrary period thickness distributions," *Proc. SPIE* **5**, 124–134 (2004).
20. H. A. Macleod, *Thin-Film Optical Filters*, Institute of Physics, Bristol (2010).
21. J. Roth et al., *Data on Low Energy Light Ion Sputtering*, IPP, 9, 26, Max-Planck-Institut für Plasmaphysik, Garching (1979).
22. Y. Yamamura and K. Muraoka, "Over-cosine angular distributions of sputtered atoms at normal incidence," *Nucl. Instrum. Methods Phys. Res. Sect. B* **42**(2), 175–181 (1989).
23. W. Schmid, "Construction of a sputtering reactor for the coating and processing of monolithic U-Mo nuclear fuel," Doctoral Dissertation, Technische Universität München (2011).
24. E. Spiller, *Soft X-Ray Optics*, SPIE Press, Bellingham, Washington (1994).
25. B. Yu et al., "Low-stress and high-reflectance Mo/Si multilayers for EUVL by magnetron sputtering deposition with bias assistance," *Appl. Opt.* **56**(26), 7462–7468 (2017).

Shizhuang Sun received his BS degree in atomic and molecular physics from the University of Science and Technology of China, and a PhD in optics from Changchun Institute of Optics, Fine Mechanics and Physics, Chinese Academy of Sciences (CIOMP). He is currently studying in the area of extreme ultraviolet optical coating technology, mainly in the Mo/Si multilayer coating deposition model.

Chunshui Jin received his BS degree in optical instrument engineering from Zhejiang University; his MS and PhD degrees in optics from CIOMP. He is working as a processor in CIOMP and involved mainly in the area of UV, EUV/soft x-ray optical technology.

Bo Yu received his BS and MS degrees in electronic science and technology from Harbin Institute of Technology and PhD in optics from CIOMP. He is currently working as an associate research fellow in CIOMP, majoring in the area of EUV/soft x-ray multilayer film.

Tao Guo received his MS degree in materials science and engineering from Southwest Jiaotong University. He is currently working at CIOMP. His work focuses on extreme ultraviolet coating technology.

Shun Yao received his MS degree in optics from Harbin Institute of Technology. He is currently working as a research assistant in CIOMP. His work focuses on optical coating process technology.

Wenyuan Deng received his PhD in condensed matter physics from CIOMP. He is currently working as an associate research fellow at CIOMP. His work focuses on optical coating process technology.

Chun Li received her BS degree in physics from Jilin University. She is currently working as an associate research fellow in CIOMP, mainly in the area of optical coating process technology.

Downloaded From: https://www.spiedigitallibrary.org/journals/Optical-Engineering on 23 Jun 2020
Terms of Use: https://www.spiedigitallibrary.org/terms-of-use